Effect of Intermolecular Forces on the Static and Dynamic Performance of Air Bearing Sliders: Part I – Effect of initial excitations and slider form factor on the stability.

Vineet Gupta

Graduate Student

Department of Mechanical Engineering

University of California, Berkeley

email: vineet@cml.me.berkeley.edu

David B Bogy

William S. Floyd, Jr., Distinguished Professor in Engineering

Department of Mechanical Engineering

University of California, Berkeley

email: dbogy@cml.me.berkeley.edu

ABSTRACT

The mechanical spacing between the slider and the disk has to be reduced to less than 5 nm in order to achieve an areal density of 1Tbit/in^2. Certain physical phenomena, such as those that can be caused by intermolecular and surface forces, which do not have a significant effect at higher flying heights, become more important at such low head-media separations. These forces are attractive for head-media separation as low as 0.5 nanometers, which causes a reduction in the mechanical spacing as compared to what would be the case without them. Single degree of freedom models have been used in the past to model these forces, and these models have predicted unstable flying in the sub-5 nm flying height range. Changes in the pitch and the roll angles were not accounted for in such models. A 3-DOF air bearing dynamic simulator model is used in this study to investigate the effect of the intermolecular forces on the static and dynamic performance of the air bearing sliders.

It is seen that the intermolecular forces increase the level of flying height modulations at low flying heights, which in turn results in dynamic instability of the system similar to what has also been observed in experiments. The effect of initial vertical, pitch and roll excitations on the static and dynamic flying characteristics of the slider in the presence of the intermolecular forces has also been investigated. A stiffness matrix is defined to characterize the stability in the vertical, pitch and roll directions. The fly height diagrams are used to examine the multiple equilibriums that exist for low flying heights. Finally, a study was carried out to compare the performance of pico and femto designs based on the hysteresis observed during the touchdown-takeoff simulations.

NOMENCLATURE

The values in the parentheses are the typical values used in this study.

C, D	: constants for atoms in vacuum (10^{-77} Jm^6, 10^{-134} Jm^{12})
U(z)	: Total pair potential
ρ_1, ρ_2	: the number densities of atoms in the disk and the slider respectively
A	: Hamaker constant, $A = \pi^2 C \rho_1 \rho_2$ (10^{-19} J)
B	: Constant, $B = \pi^2 D \rho_1 \rho_2$ (10^{-76} Jm^6)
z	: fly height, nm
θ	: pitch angle, μrad
φ	: roll angle, μrad
m	: slider's mass, gm
I_θ, I_φ	: slider's moments of inertia in pitch and roll directions, respectively
F_{su}	: suspension pre load, gm
F_c	: contact force, gm
F_{vdw}	: intermolecular force, gm
$M_{su\theta}$, $M_{su\varphi}$	: moment in the pitch and roll directions due to suspension preload
$M_{sh\theta}$, $M_{sh\varphi}$	: moment in the pitch and roll directions due to shear force
$M_{c\theta}$, $M_{c\varphi}$	: moment in the pitch and roll directions due to contact force
$M_{vdw\theta}$, $M_{vdw\varphi}$	: moment in the pitch and roll directions due to intermolecular force
p	: air pressure, Pa
p_a	: ambient pressure, Pa (1.01325×10^5 Pa)
P	: dimensionless air pressure, p/p_a

H	: dimensionless bearing clearance, h/h_m
X	: dimensionless coordinate in slider length direction, x/L
Y	: dimensionless coordinate in slider width direction, y/L
h_m	: reference clearance at the trailing edge center, nm
L	: length of the slider, mm
Λ_x	: bearing number in x direction, $6\mu UL/p_a h_m^2$
Λ_y	: bearing number in y direction, $6\mu VL/p_a h_m^2$
σ	: squeeze number, $12\mu\omega L^2/p_a h_m^2$
Q	: flow factor, assumes different forms depending on the type of slip model used
F	: total force in z direction
T_θ, T_φ	: total torque in the pitch and roll directions, respectively
ID, MD, OD	: Inner diameter, middle diameter and outer disk diameters, respectively

INTRODUCTION

Dynamic instability has been observed experimentally for ultra low flying sliders. Various head disk interface (HDI) models that have been used so far, are unable to explain this instability. Thus it is important to consider certain physical phenomena like dispersion forces in modeling flying characteristics for ultra low separations at the HDI. Wu and Bogy [1,3] have shown that there is a reduction in fly height due to intermolecular forces (IMF) for sub 5nm flying sliders. Earlier a single degree of freedom model was used by Thornton and Bogy [2] to predict instability due to these forces at the HDI. A parametric study was conducted to predict the dynamic instability caused by the double well potential system causing strange attractors and leading to chaotic high amplitude oscillations of the slider [4,8]. However these models were unable to capture the complex dynamic instability as the dependence on the pitch and roll angles were not considered. A 3-DOF air bearing model is used in this study to investigate the effect of intermolecular forces.

These forces, like gravitational forces, act between all atoms and molecules, even if they are neutral. The attractive forces acting between two neutral molecules postulated by van der Waals may be practically understood from a classical electrical point of view. If the two molecules carry dipole moments they will mutually influence their spatial orientations in such a way that, on average, there is an attractive force. Moreover, each molecule induces a dipole in the other molecule and the attraction is reinforced by this mutual polarization. These universal attractive forces acting between all atoms, molecules, ions, etc. have been explained on the basis of wave mechanics. They may be understood as being the result of the mutual influencing of the electronic motion in the two atoms under consideration. This temporary dipole in one atom induces a dipole in the second atom, and the result is attraction. Inversely, the fluctuating dipole in the second atom induces a dipole in the first atom [7].

There are also strong repulsive forces at very small interatomic distances, which determine how close two atoms or molecules can approach each other. These repulsive forces are due to an overlap of the electron clouds of atoms. They are short range forces and increase sharply as the two molecules come together.

The total pair potential is obtained by summing the attractive and the repulsive potentials. The Lennard-Jones or '6-12' potential is used in this study to model the total pair potential due to attractive and repulsive forces.

INTERMOLECULAR FORCE BETWEEN TWO LAYERS

In order to calculate the van der Waals interaction energies in vacuum for a pair of bodies of different geometries, we assume that the interaction is non-retarded and additive. We know that the interatomic van der Waals pair potential is of the form

$$U(z) = -C / z^6 + D / z^{12} \qquad (1)$$

We integrate the energies of all the atoms in one body with respect to all the atoms in the other and thus obtain the two body potential per unit area of one surface interacting with an infinite area of another surface

$$U(z) = -\frac{\pi C \rho_1 \rho_2}{12 z^2} + \frac{\pi D \rho_1 \rho_2}{360 z^8} \qquad (2)$$

where ρ_1 and ρ_2 are the number densities of atoms in the disk and the slider, respectively. This equation can be alternatively written as

$$U(z) = -\frac{A}{12\pi z^2} + \frac{B}{360\pi z^8} \qquad (3)$$

in terms of the Hamaker constants (A) and another constant (B), where $A = \pi^2 C \rho_1 \rho_2$ and $B = \pi^2 D \rho_1 \rho_2$. Typical values for A and B are about 10^{-19} J and 10^{-76} Jm^6, respectively.

The total interaction energy between the slider and the disk, obtained by integrating the above expression over the whole slider surface, is given by

$$U_{tot}(z) = -\frac{A}{12\pi} \iint_{\substack{Rect \\ area}} \frac{dxdy}{z^2} + \frac{B}{360\pi} \iint_{\substack{Rect \\ area}} \frac{dxdy}{z^8} \qquad (4)$$

And the intermolecular forces between the slider and the disk can be written as

$$F_{vdw} = \frac{d(U_{tot})}{dz} = -\frac{A}{6\pi} \iint_{\substack{Rect \\ area}} \frac{dxdy}{z^3} + \frac{B}{45\pi} \iint_{\substack{Rect \\ area}} \frac{dxdy}{z^9} \qquad (5)$$

INTERMOLECULAR FORCE MODELING

When the slider is flying at low mechanical separations the forces acting on the slider at the HDI are the suspension force, air bearing force, contact force, shear force and the intermolecular force.

To calculate the static flying characteristics of the air bearing slider, we considered a three DOF model in the variables fly height (z), pitch (θ) and roll (φ). The following force and moment balance equations are used to model the HDI

$$\begin{aligned} m\frac{d^2z}{dt^2} &= F_{su} + F_c + F_{vdw} + \int (p - p_a)dA \\ I_\theta \frac{d^2\theta}{dt^2} &= M_{su\theta} + M_{sh\theta} + M_{c\theta} + M_{vdw\theta} + \int (p - p_a)(x_g - x)dA \\ I\varphi \frac{d^2\varphi}{dt^2} &= M_{su\varphi} + M_{sh\varphi} + M_{c\varphi} + M_{vdw\varphi} + \int (p - p_a)(y_g - y)dA \end{aligned} \qquad (6)$$

The relationship between the pressure distribution and the HDI spacing is given by the generalized Reynolds equation:

$$\frac{\partial}{\partial X}\left(QPH^3\frac{\partial P}{\partial X} - \Lambda_x PH\right) + \frac{\partial}{\partial Y}\left(QPH^3\frac{\partial P}{\partial Y} - \Lambda_y PH\right) = \sigma\frac{\partial}{\partial t}(PH) \qquad (7)$$

These equations are used to calculate the dynamic response of the air bearing slider. The Quassi-Newton iteration method is implemented to calculate the static solutions, the case where all the time dependent terms are zero.

STABILITY CRITERIA FOR THE HDI

For stability at the HDI, the total stiffness in the vertical, pitch and roll directions must be positive. In other words the total bearing load capacity must be positive. It has been found that at ultra low fly heights the stiffness decreases as the fly height decreases and becomes negative below a critical fly height value [5]. Negative stiffness means that the bearing is unable to maintain a mechanical spacing between the slider and the disk, which implies that contact will occur between the slider and the disk.

The stiffness matrix relating changes in the forces in the z direction and moments in the pitch and roll directions to changes in the fly height (z), pitch (θ) and roll (φ) can be mathematically represented as

$$\begin{bmatrix} dF \\ dT_\theta \\ dT_\varphi \end{bmatrix} = \begin{bmatrix} \frac{\partial F}{\partial z} & \frac{\partial F}{\partial \theta} & \frac{\partial F}{\partial \varphi} \\ \frac{\partial T_\theta}{\partial z} & \frac{\partial T_\theta}{\partial \theta} & \frac{\partial T_\theta}{\partial \varphi} \\ \frac{\partial T_\varphi}{\partial z} & \frac{\partial T_\varphi}{\partial \theta} & \frac{\partial T_\varphi}{\partial \varphi} \end{bmatrix} \begin{bmatrix} dz \\ d\theta \\ d\varphi \end{bmatrix} \quad (8)$$

The system is stable only if it is stable in all three directions, i.e. z, pitch and roll. Mathematically, if all three eigenvalues of the stiffness matrix are positive, then the system is stable. But if one or more of the eigenvalues of the stiffness matrix are negative, then the system is unstable.

STABILITY PREDICTION USING THE FLY HEIGHT DIAGRAM

In this study the stability/instability of the HDI is analyzed using a "fly height diagram". The fly height diagram plots the slider fly height versus the disk rpm. The minimum mechanical spacing between the slider and the disk is referred to as the fly height. A typical fly height diagram is shown in fig.1. The points on curve 1 give the steady state fly height vs disk rpm without considering the effect of intermolecular forces. All the points on this curve have positive stiffness values and hence are stable.

The curves 2 and 3 plot the variation of the fly height versus disk rpm taking into consideration the effect of intermolecular forces. From the figure we observe multiple equilibrium points for disk rpm's between 1900 and 4300. The equilibrium points on the curve 2 have positive stiffness values and hence are stable equilibrium points. However the points on the curve 3 have negative stiffness values and hence are unstable equilibrium points.

From the fly height diagrams we observe that as the disk rpm decreases from 12000 to as low as 1900, a stable fly height is given by the curve 2. Below 1900 rpm (corresponding to a fly height of 3.4nm) the slider becomes unstable and contact occurs between the slider and the disk. This value of disk rpm gives the touchdown rpm. If the disk rpm is increased from 1900, the slider remains unstable until a disk rpm of 4300. This is because at a disk rpm of 1900 the slider is in contact with the disk. This means that the slider is initially disturbed from its stable equilibrium position (curve 2) and hence it will oscillate between the multiple equilibriums that exist until a disk rpm of 4300. For rpm's above 4300 (corresponding to a fly height of 5.05nm) there is only one equilibrium point, which is stable and hence the stability of the HDI is restored at 4300. This value of rpm gives the takeoff rpm. The stable fly height for the system is 5.05 nm

above which the system will always converge to a stable equilibrium if it is perturbed about its steady state due to external disturbances such as air flow, disk roughness etc. We call this fly height the "desired fly height" later on.

From this discussion we conclude that the rpm range of the curve 2 in the fly height diagram gives an estimate of the hysterisis observed in touchdown-takeoff experiments. We can also conclude that the larger the range of the unstable region (curve 2), the more will be the hysterisis observed in the touchdown-takeoff experiments.

RESULTS

Static simulations were carried out at 7200 rpm for the slider design shown in fig.2 at three different radial positions. The fly height, pitch and roll, with and without intermolecular forces, are shown in Table 1. We observe that the fly height value is slightly reduced when intermolecular forces are considered, which is expected as the intermolecular forces are attractive in nature. But since the fly heights are more then 10 nm, the reduction in fly height is not much, as the attractive intermolecular forces are very weak at such large separations. We also observe that the intermolecular forces slightly increase the magnitude of the pitch and roll angles.

Static simulations were also carried out at 3500 disk rpm for the slider design shown in fig.3 at three different radial positions. The fly height, pitch and roll with and without intermolecular forces are shown in Table 2. Since this is a relatively low flying slider, there is significant reduction in the fly height due to the intermolecular forces. Due to the attractive nature of the intermolecular forces their inclusion reduces the fly height at all three radial positions. Fig. 4 shows that the magnitude of the intermolecular force is maximum at the OD and minimum at the MD radial position and hence there is a maximum reduction in the fly height at the OD and minimum reduction at the MD radial position. We also observe that the intermolecular forces slightly increase the magnitude of the pitch and roll angles.

Fig. 5 plots the variation in intermolecular force, air bearing force and total force as the fly height changes at the ID radial position. We observe that the total force equals the suspension preload of 1.5gm at three different fly heights. This implies the existence of three equilibrium fly heights at the disk rpm of

3500. But the third equilibrium occurs at just 0.2nm, and HDI spacing below the inter-atomic separation of 0.2nm is considered contact. Hence the third equilibrium cannot exist for stable flying conditions.

Fig. 6 shows the dynamic response without and with intermolecular forces at a disk rpm of 3500, at the three radial positions for some initial excitations. The solver converges to a stable fly height when the intermolecular forces are not considered, but the inclusion of the intermolecular forces results in large fly height modulations, which implies instability of the system. Dynamic simulations were also carried out with intermolecular forces at the disk rpm of 7200 as shown in fig.7. The solver converges to a stable fly height value at this disk rpm.

The fly height diagrams for the slider shown in fig. 3 are plotted in fig. 8 for three different radial positions. We observe that at the disk rpm of 3500, there exist multiple equilibrium point's at all three radial positions. Hence the simulations started with some perturbation about the steady state results in large modulations in fly height as shown in fig. 6. However, only one (stable) equilibrium exists at a disk rpm of 7200. Hence the system always converges to a steady state for all small perturbations about the equilibrium point as shown in fig 7. We observe that the rpm range of the unstable region is least at the outer diameter (OD) position and greatest at the inner diameter (ID) position. The desired fly height, beyond which there exists only one equilibrium, also decreases from ID (6.07nm) to MD (5.07nm) to OD (3.57nm) as shown in Table 3.

To analyze the effect of slider form factor on dynamic stability, we carried out static simulations for both the pico and femto designs at the same radial positions, for the slider designs shown in fig. 9. The pico slider was simulated with 1.5gm suspension load and the femto slider was simulated with 0.75gm and 1.5gm suspension load. The fly height diagrams are shown in fig.10. We observe that the pico design has the least unstable rpm range from a disk rpm of 3000 to 4500. Hence we can predict that less hysterisis will be observed with the pico design as compared to the femto design in touchdown-takeoff experiments. The desired fly heights for the three cases are also shown in Table 3. The femto design with 1.5gm suspension load has lowest desired fly height of 3.37 nm. If we compare the results for the two femto designs, we observe that on increasing the gram load from 0.75gm to 1.5gm the desired fly height value decreases from 4.15 nm to 3.37 nm, but we need to spin the disk at higher rpm's to attain this fly height.

Simulations were also carried out for pico and femto designs at the same radial positions for the slider designs shown in fig. 11. The pico slider was simulated with a 1.9gm suspension load and the femto slider was simulated with 0.75gm and 1.9gm suspension loads. The multi-equilibrium regions are shown using the fly height diagram in fig.11. We again observe that the pico design has a smaller unstable rpm range from 7700 to 10100, hence less hysterisis will be observed with the pico design as compared to the femto design in touchdown-takeoff experiments. The desired fly heights for the three cases are shown in Table 4. The femto design with 1.9gm suspension load has lowest desired fly height of 6.20 nm. If we compare the results for the two femto designs, we again observe that on increasing the gram load from 0.75gm to 1.9gm the desired fly height value decreases from 11.79 nm to 6.20 nm, but we need to spin the disk at higher rpm's to attain this fly height.

From the above simulation results we conclude that smaller hysterisis will be observed with pico designs when conducting touchdown-takeoff simulations. But smaller stable fly heights can be obtained with femto designs at higher suspension preloads. The effect of suspension preload on the desired fly height and the HDI stability will be discussed in the Part II paper.

CONCLUSIONS

Intermolecular forces have been included in the CML static and dynamic air bearing design programs. Static and dynamic simulations are carried out with and without considering the intermolecular forces. Due to the attractive nature of the intermolecular forces, a reduction in fly height value is observed when these forces are included. These forces also increase the magnitude of the pitch and roll angles slightly. At low disk rpm's there exists three equilibrium points, one of which corresponds to contact at the HDI. Among the two equilibrium points that can exist at low disk rpm's, one is stable and the other one is unstable. If the slider is perturbed from its stable equilibrium position in the bi-equilibrium region, it will undergo large excursions. From the simulations carried out to analyze the effect of slider form factor, it can be concluded that pico designs will have smaller hysterisis when compared to femto designs during touchdown-takeoff simulations. But smaller stable fly heights can be obtained with femto designs at higher suspension preloads.

ACKNOWLEDGMENTS

This work was supported by the Computer Mechanics Laboratory at the University of California, Berkeley.

REFERENCES

[1] Wu. L., "Physical modeling and numerical simulations of the slider air bearing problems in hard disk drives," Ph.D. dissertation, University of California, Berkeley, 2001

[2] Thornton B.H., "Head-Disk Interface Dynamics of Ultra-Low Flying Air Bearing Sliders for Hard-Disk Drive Applications," Ph.D. dissertation, University of California, Berkeley, 2003

[3] Lin Wu, Bogy DB., "Effect of the intermolecular forces on the flying attitude of sub-5 nm flying height air bearing sliders in hard disk drives," Transactions of the ASME, Journal of Tribology, vol.124, no.3, July 2002, pp.562-7.

[4] Thornton BH, Bogy DB, "Head-disk interface dynamic instability due to intermolecular forces," IEEE Transactions on Magnetics, vol.39, no.5, pt.2, Sept. 2003, pp.2420-2.

[5] B. Zhang, and A. Nakajima, "Possibility of surface force effect in slider air bearings of 100 Gbit/in 2 hard disks," Tribology International, vol. 36, pp. 291-296, April – June 2003.

[6] J. H. Li, B. Liu, W. Hua, and Y. S. Ma, "Effects of intermolecular forces on deep sub- 10 nm spaced sliders," IEEE Trans. Magn , vol. 38, pp. 2141-2143, Sept. 2002.

[7] J. N. Israelachvili, Intermolecular and surface forces, 2nd ed. San Deigo: Academic Press, 1992.

[8] B. H. Thornton, and D. B. Bogy, "Non-Linear Aspects of Air Bearing Modeling and Dynamic Spacing Modulation in Sub 5 nm Air Bearings for Hard Disk Drives," IEEE Transaction on Magnetics, Vol. 39, pp. 722-728, March 2003.

[9] Bogy DB, Fong W, Thornton BH, Hong Zhu, Gross HM, Bhatia CS, "Some tribology and mechanics issues for 100-Gb/in/sup 2/ hard disk drive," IEEE Transactions on Magnetics, vol.38, no.5, pt.1, Sept. 2002, pp.1879-85.

Table 1: Effect of the intermolecular force on the static performance of the pico slider (fig. 2)

	Fly Height (nm)			Pitch (μrad)		Roll (μrad)	
	w/o IMF	with IMF	% reduction in fly height	w/o IMF	with IMF	w/o IMF	with IMF
ID	12.0051	11.984	0.18	248.64	248.67	-0.32	-0.38
MD	11.3949	11.3624	0.29	266.93	267.16	-1.98	-2.06
OD	10.8077	10.7721	0.33	267.53	267.73	-7.11	-7.22

Table 2: Effect of the intermolecular force on the static performance for the pico slider (fig. 3)

	Fly Height (nm)		Pitch (μrad)		Roll (μrad)	
	w/o IMF	with IMF	w/o IMF	with IMF	w/o IMF	with IMF
ID	6.1842	5.6167	95.03	96.03	-2.37	-2.39
MD	5.1152	4.7458	124.18	124.79	3.70	3.88
OD	3.0852	2.4398	146.00	146.92	6.68	7.55

Table 3: Touchdown-takeoff rpm's and desired fly height

	Touchdown RPM	Takeoff RPM	Hysterisis in RPM	Desired Fly Height (nm)
Pico w 1.5gm	3000	4500	1500	3.57
Femto w 0.75gm	3000	7000	4000	4.15
Femto w 1.5gm	5800	10500	4700	3.37

Table 4: Touchdown-takeoff rpm's and desired fly height

	Touchdown RPM	Takeoff RPM	Hysterisis in RPM	Desired Fly Height (nm)
Pico w 1.9gm	7700	10100	2400	11.90
Femto w 0.75gm	7300	10700	3400	11.79
Femto w 1.9gm	12700	15500	2800	6.20

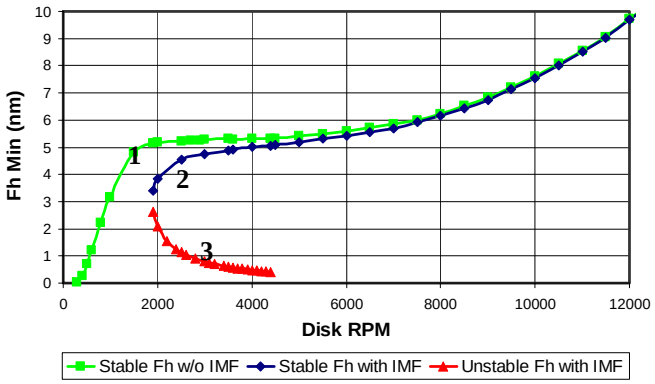

Fig. 1 Fly height diagram

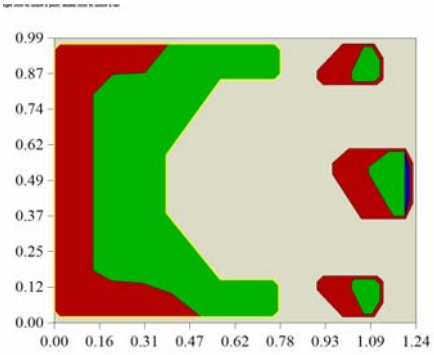

Fig. 2 Pico slider with a crown of 30 nm and a camber of -5 nm. The base recess is 1.397 μm.

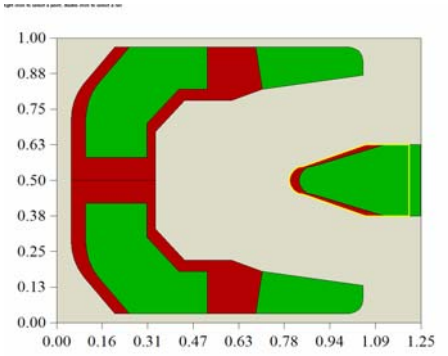

Fig. 3 Pico slider with a crown of 25.4nm and a camber of 2.5nm. The base recess is 2.5μm.

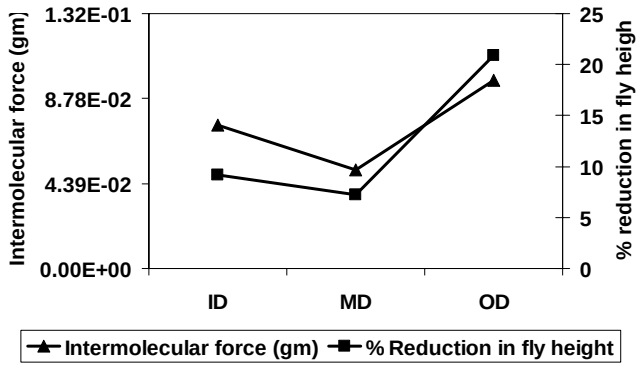

Fig. 4 Intermolecular force magnitude and percentage reduction in fly height at three different radial positions.

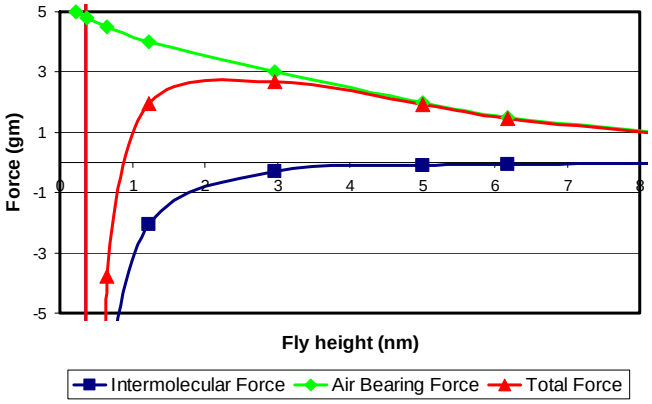

Fig. 5 Intermolecular force, air bearing force and total force versus fly height

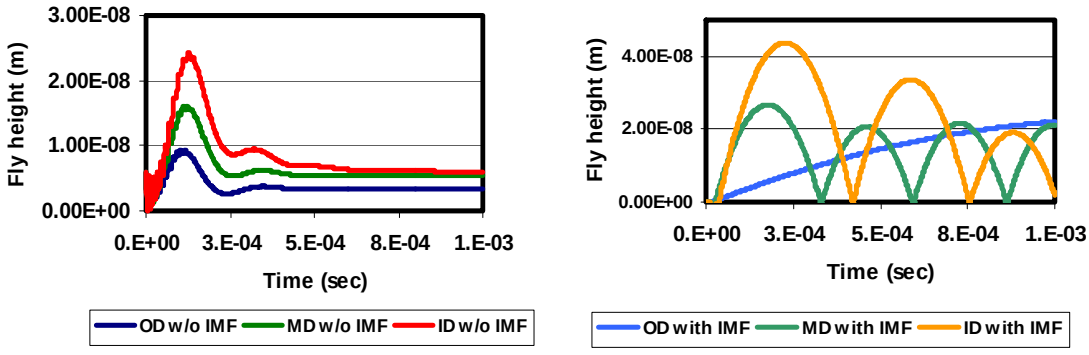

Fig. 6 Dynamic response without and with intermolecular forces at a disk rpm of 3500.

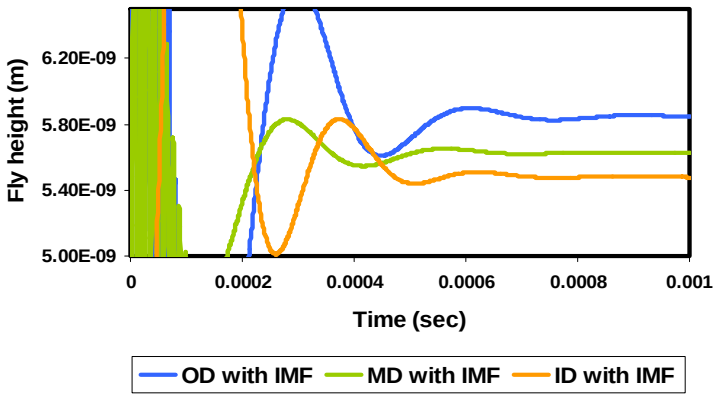

Fig. 7 Dynamic response with intermolecular forces at a disk rpm of 7200.

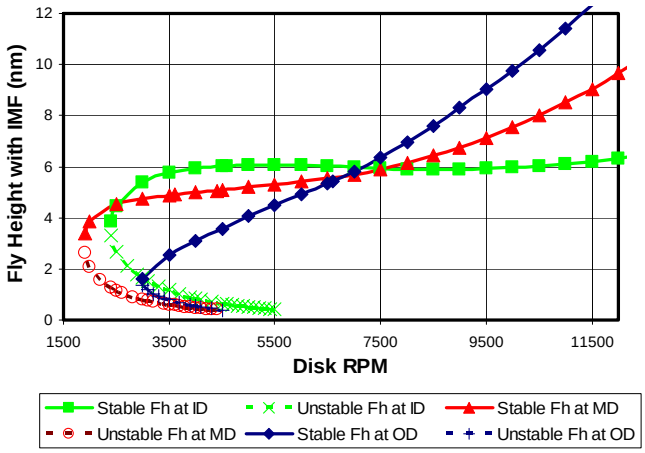

Fig. 8 Fly height diagram for slider shown in fig. 3

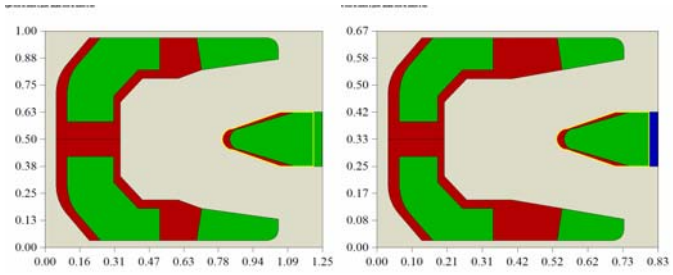

Fig.9 Pico slider with a crown of 25.4nm and a camber of 2.5nm. The base recess is 2.5µm. Femto slider with a crown of 17nm and a camber of 2nm. The base recess is 2.3µm.

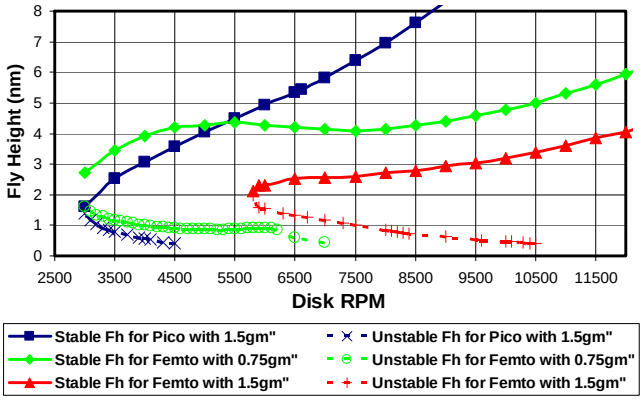

Fig. 10 Fly height diagrams for pico and femto slider designs at different suspension preloads.

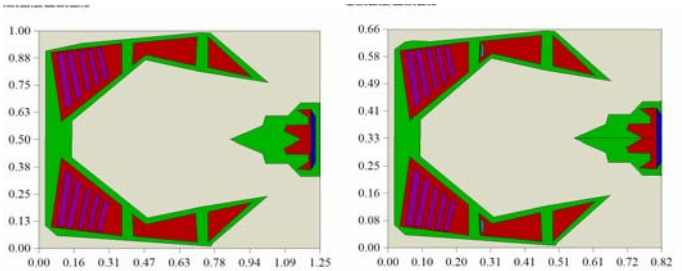

Fig.11 Pico slider with a crown of 25.4nm and a camber of 2.5nm. The base recess is 2.5µm.

Femto slider with a crown of 17nm and a camber of 2nm. The base recess is 2.5µm.

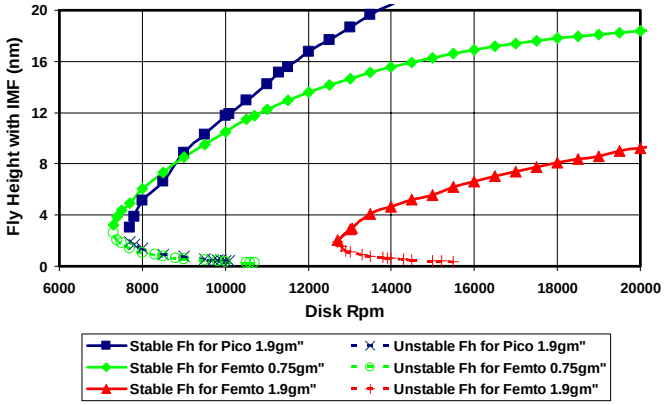

Fig. 11 Fly height diagrams for pico and femto slider designs at different suspension preloads.